JOURNAL OF SPACECRAFT AND ROCKETS
Vol. 33, No. 5, September–October 1996

Space Station Based Tethered Interferometer for Natural Disaster Monitoring

Antonio Moccia*
University of Naples "Federico II," 80125 Naples, Italy
and
Marco D'Errico† and Sergio Vetrella‡
Second University of Naples, 81031 Aversa (CE), Italy

A synthetic aperture radar interferometer based on two vertically spaced physical antennas carried along parallel paths by the Space Station and by a small tethered subsatellite is presented. This remote sensing system is aimed at producing and updating topographic maps. In particular, it offers geometric, radiometric, and temporal resolutions adequate for natural-disaster monitoring. The system performance is identified by means of a computer simulation, taking account of the tethered platform dynamics and of the Space Station orbital decay. Numerical results show the capability of observing any point of the Earth surface in the range of latitudes ±51.6 deg with a repetitivity of about 2 days, by using range steering of the antenna beams (15–45 deg). Then, the attitude pointing accuracy requirements are derived by evaluating the signal-to-noise ratio and the swath overlap decrease due to the antenna misalignment (yaw 0.15 deg, pitch 0.10 deg, roll 0.20 deg).

Nomenclature

A = resolution element area, m^2
a = orbit semimajor axis, km
B_z = vertical separation of antennas (baseline z component), km
E = number of Earth rotations in the repetition period
f_D = Doppler centroid frequency, Hz
G = antenna gain, dB
G_R = range compression factor, dB
h = topographic height, m
INT = truncation to integer
i = orbit plane inclination, deg
N = noise, dB
N_L = number of radar looks
P_p = peak power, dB
Q = orbit repetition factor
R = slant range, km
$R_\oplus$ = Earth radius, km
$\boldsymbol{R}$ = slant range vector, km
$\dot{\boldsymbol{R}}$ = time derivative of slant range vector, km/s
S = number of satellite revolutions in the repetition period
S_W = radar swath width, km
T_A = azimuth integration time, s
β = mean anomaly in the orbit plane, deg
γ = yaw attitude angle, deg
ΔW_A = Doppler bandwidth, Hz
ϑ = antenna pointing angle (off nadir), deg
λ = wavelength, cm
σ_h = height measurement accuracy, m
σ_ϕ = phase-difference measurement accuracy, rad
σ_0 = terrain backscatter cross section, dB
ϕ = phase difference in the interferogram, rad
ω = satellite angular velocity, deg/s
$\omega_\oplus$ = Earth angular velocity, deg/s

Received June 8, 1995; revision received March 28, 1996; accepted for publication May 20, 1996.

*Professor of Spacecraft Attitude Dynamics and Control, Dipartimento di Scienza e Ingegneria dello Spazio Luigi G. Napolitano, P. le Tecchio 80. Member AIAA.

†Staff Scientist, Dipartimento di Ingegneria Aerospaziale, Real Casa dell' Annunziata. Member AIAA.

‡Professor of Space System Engineering, Dipartimento di Ingegneria Aerospaziale, Real Casa dell'Annunziata.

Introduction

IT is well known that synthetic aperture radar (SAR) interferometry allows the three-dimensional observation of the Earth surface, thanks to the phase difference in the signals received by two radar antennas separated by a distance called the baseline.[1] In recent years several authors have demonstrated that spaceborne SAR interferometry is a successful topographic mapping technique. It offers a high-resolution image and a high-accuracy digital elevation model (DEM).[2]

Among the various proposed applications of topographic mapping to Earth sciences (hydrology, ecology, geomorphology, ice sheets and glaciers, geology, geophysics),[3–5] there is the possibility of getting a DEM with an accuracy adequate for natural-disaster monitoring. In natural-disaster management, three main goals can be identified: preparedness, prevention, and relief. Preparedness consists of the minimization of losses when a disaster strikes; in prevention one tries to avoid or control hazards; and in relief aid is provided after a disaster occurs. As an example, Earth surface volumetric changes and small crustal motions are premonitory events of natural disasters such as floods, landslides, avalanches, volcanic eruptions, and earthquakes and can be detected by differential SAR interferometry techniques.[6,7] On the other hand, the possibility of producing and updating SAR images and topographic maps in nearly real time can be useful in natural-disaster relief, because these data could allow a more effective intervention: identification of evacuation routes, sites of temporary dwellings, sources of water.[8] Furthermore, active microwave sensors are not affected by clouds, precipitation, and local time.

Spaceborne remote sensing applications to disaster management are strongly limited by a tradeoff between spatial and temporal resolutions. Existing satellites (e.g., meteorological satellites) achieve high temporal resolution by decreasing spatial resolution. On the other hand, because of orbital and data-rate constraints, remote sensing satellites can accomplish high geometric resolution only at the expense of swath width and repetitivity.

Besides its high topographic accuracy, SAR interferometry offers the possibility of overcoming the temporal resolution constraints through its capability of antenna range beam steering.[9] In fact, it is possible to get a high frequency of observation over areas hit by natural disasters by moving the nominal swath width within a wider off-nadir area.

Despite the great potential of observation from space, satellites have rarely been designed for natural-disaster monitoring: in recent years a small satellite mission[10] and a European retrievable

carrier (EURECA) experiment[11] have been proposed for monitoring volcano gaseous emissions. Nevertheless, the need of a large-swath, high-observation-frequency, long-lifetime spaceborne system is more and more evident, to furnish accurate, real-time input data to a global natural-disaster management system.

The main goal of this paper is to present a new SAR interferometer based on two tethered antennas. In particular, the system is aimed at the high-frequency and high-resolution topographic mapping of areas hit by natural disasters. The gravity-gradient-stabilized configuration consists of a transmitting/receiving antenna onboard the Space Station, and a receiving-only antenna carried by a small tethered subsatellite.

Furthermore, the system can take advantage of the unique capabilities offered by the Space Station, such as a mission lifetime adequate for an operational natural-disaster monitoring system. In addition, extensive onboard data handling and processing before transmission allows a simplification of SAR design and operation and a significant reduction of data rate. As an example, only the compressed and calibrated images and the DEMs need be downlinked, and that can be done in nearly real time by means of the already scheduled Data Relay Satellites constellation. Moreover, active microwave sensors do not need sun-synchronous orbits or very stringent platform attitude requirements. The sensor under study could be part of a permanent tethered facility on board the Space Station: in fact, a large number of Space Station based tethered system applications have been proposed in recent years.[12]

After a brief introduction to the main factors affecting the height measurement accuracy of a SAR interferometer, this paper deals with the evaluation of the observation repetitivity achievable by using range-steerable antennas. Although a comprehensive study of natural-disaster management by means of spaceborne remote sensing is not yet available, it is evident that the required geometric, radiometric, and temporal resolutions strongly depend on the observed phenomena. For the sake of concreteness, this paper is focused on the resolution and repetitivity adequate for monitoring the campi Flegrei (Naples, southern Italy) area bradyseism and volcanism. In particular, the area bradyseism is characterized by small vertical movements of the order of few centimeters per year. Generally, before the movement inversion, the velocity of rising strongly increases up to few centimeters per month. During the years 1969–1970, the maximum value of 6 cm/month was recorded. Other gathered data show that the Mt. Nuovo volcano flanks rose up to 5 m in a few days before the explosive eruption.

Finally, the effects of the space system dynamics on SAR performance are studied to evaluate the tether effects and to derive the attitude accuracy requirements. The analysis has been carried out by means of a computer code that the authors developed for spaceborne interferometric SAR simulation. It allows for Keplerian or perturbed orbits, attitude control and maneuver, SAR pointing geometry and radiometric characteristics, various antenna configurations, Earth ellipsoid, terrain morphology, and surface backscattering characteristics.

Vertical SAR Interferometry

The past and existing space missions achieve SAR interferometry by using two images of the same area obtained by the same antenna, during cross-track separated coverages (repeat-orbit interferometry). In this case, the two images forming the interferogram are acquired at different times, which causes a major limitation: time decorrelation.[2,13]

To avoid this limitation the two images must be acquired simultaneously by means of two antennas, which can operate on a single spacecraft or on different platforms. In the first case, a quite large boom is mandatory, which causes several complexities and difficulties in system design and operation. In the second case, two solutions can be envisaged: a horizontal baseline (achieved by using two free satellites at the same altitude and inclination with slightly separated ascending nodes[14,15]) and a vertical baseline (obtained if the two satellites are connected by a tether[16]). It has been demonstrated that these systems are adequate for global topographic mapping at an accuracy that meets the 1:50,000 scale standards.

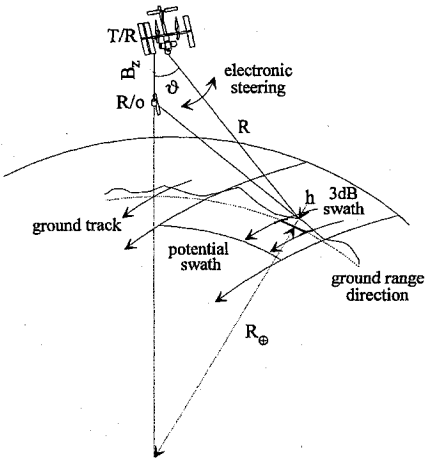

Fig. 1 Tethered interferometric SAR observation geometry.

With reference to the observation geometry of a tethered vertical interferometer (Fig. 1), by means of the complex images acquired by the transmitting/receiving (T/R) and the receiving-only (R/o) antennas it is possible to calculate the height as follows:

$$h = (a^2 + R^2 - 2Ra\cos\vartheta)^{\frac{1}{2}} - R_\oplus \tag{1}$$

where the off-nadir angle is related to the phase difference in the interferogram:

$$\phi = (2\pi/\lambda)B_z\cos\vartheta \tag{2}$$

From Eqs. (1) and (2), assuming that systematic errors have been essentially removed by some small set of ground control points, and considering uncorrelated parameters, it is possible to derive quantitatively the effect on the height measurement accuracy of the uncertainties in the determination of phase difference, baseline, and slant range.[1,2,4,16] In particular, the slant range error is centimetric, because it is caused by the clock timing error and the atmospheric delay, and it can certainly be neglected. The baseline uncertainty depends on the measurements technique, and it can be strongly reduced by adopting differential Global Positioning System (GPS) and/or laser ranging sensors. Consequently, the major contribution to the height measurement uncertainty is caused by the interferometric phase uncertainty as follows:

$$\sigma_h = \frac{\lambda a R}{2\pi B_z(a^2 + R^2 - 2aR\cos\vartheta)^{\frac{1}{2}}}\sigma_\phi \tag{3}$$

Assuming large signal-to-noise ratio (SNR) and Rician statistics on the received phasors, the standard deviation of the interferometric phase can be computed as follows[13,17]:

$$\sigma_\phi \approx \frac{1}{\sqrt{N_L \cdot \mathrm{SNR}}} \tag{4}$$

Therefore, an adequate SNR must be guaranteed to attain a satisfactory height measurement accuracy.

Frequency of Observation

In repetitive orbits the ground tracks produce exactly the same pattern after each repetition period. That is, after S satellite revolutions and E Earth rotations (a repetition period), the ground track falls over the same point of the Earth's surface. The repetition factor is defined as follows:

$$Q = S/E \tag{5}$$

As shown by Duck and King,[18] in a repetition period the equator is divided into S equal parts. If global coverage is required, the projection of the radar swath on the equator must be larger than the

distance between adjacent tracks. Therefore, the minimum value of S that yields global coverage is given by

$$S_{\mathrm{MIN}} = \mathrm{INT}\left\{ \frac{2\pi}{\sin^{-1}[\sin(S_W/R_\oplus)/\sin i]} \right\} \tag{6}$$

As a consequence, the 3-dB beam aperture in range direction must be selected large enough to satisfy Eq. (6). On the other hand, to limit the data rate and to attain high geometric resolution, the 3-dB swath must be relatively small. If steerable antennas are envisaged, the potential swath can be considered instead of the 3-dB one. In this case Eq. (6) gives the minimum value of S that guarantees global access.

Although the Space Station nominal design parameters have not yet been definitively established, for the sake of concreteness, in the simulation we considered an orbit inclination of 51.6 deg and an altitude ranging between 440 and 480 km.[19] With reference to the radar characteristics (Table 1), we considered the L band because it has a proven history of use (SEASAT, SIR, JERS-1) and it is scheduled for a future global topographic mission (TOPSAT). The antenna 3-dB aperture angles coincide with the TOPSAT values, while the 1-km vertical antenna separation is a tradeoff between height accuracy and gravity gradient stabilisation.[16]

Considering the significant altitude variations of the Space Station during the decay and reboost phases, we selected a range of repetition factors (15.184–15.056) that does not necessarily offer global coverage. On the other hand, if 15–45-deg steerable antennas are considered, global access is guaranteed. Moreover, a steerable antenna greatly increases the observation frequency over selected test sites.

Table 1 SAR characteristics

Left-looking off-nadir angle	30 deg
3-dB antenna azimuth angle	1.34 deg
3-dB antenna elevation angle	3.46 deg
Wavelength	24 cm
Ground resolution	30 × 30 m^2

In a previous study[20] the authors considered six orbits at altitudes of ≈440, ≈460, and ≈480 km and off-nadir angles steerable in the ranges 25–35, 20–40, and 15–45 deg. It was demonstrated that when the off-nadir angle can be varied in the range 15–45 deg, the mean value of the time interval between successive observations of any point in the accessible latitudes (±51.6 deg) is reduced to ≈2 days.

The present study has been conducted in the whole range of Space Station altitudes, considering 161 repetitive orbits, with 51.6-deg inclination, S ranging between 91 and 19,381 and E between 6 and 1313. The altitude difference between successive orbits varies between 7.5 and 660 m. Statistical distributions of the time between successive observations have been computed, considering a large set of point targets on the Earth surface, randomly extracted in the uniform range of the accessible latitudes (±51.6 deg). In particular, the mean value, the standard deviation, and their linear regression have been computed. Figure 2 shows that the mean value slightly decreases with increasing altitude, while the standard deviation increases. This is consequent to the obvious increase of the swath at higher antenna altitudes. Moreover, thanks to the 15–45-deg antenna steering, the observation frequency practically does not depend on the repetition factor.

In conclusion, the analysis demonstrated the great potential for fast accessing of the Earth surface from the Space Station in its whole interval of operational altitudes: a mean interval of 2 days elapses between successive observations, with a standard deviation of 2 days.

Nominal Doppler Parameters

In the following, the evaluation of the nominal Doppler centroid frequency and bandwidth will be presented, because these parameters are affected by the antenna attitude and influence the coherence of the interferogram. In particular, it will be shown that the Doppler centroid frequency is strongly influenced by yaw and pitch attitude angles whereas the roll-angle effect is practically negligible. The analysis was conducted for the orbit with the repetition factor 892/59 (460 km), including also the possibility of yaw attitude angle steering. On existing satellites, the yaw attitude angle steering is performed to align the SAR antenna along the spacecraft–atmosphere relative velocity so that the atmospheric drag is reduced. In this

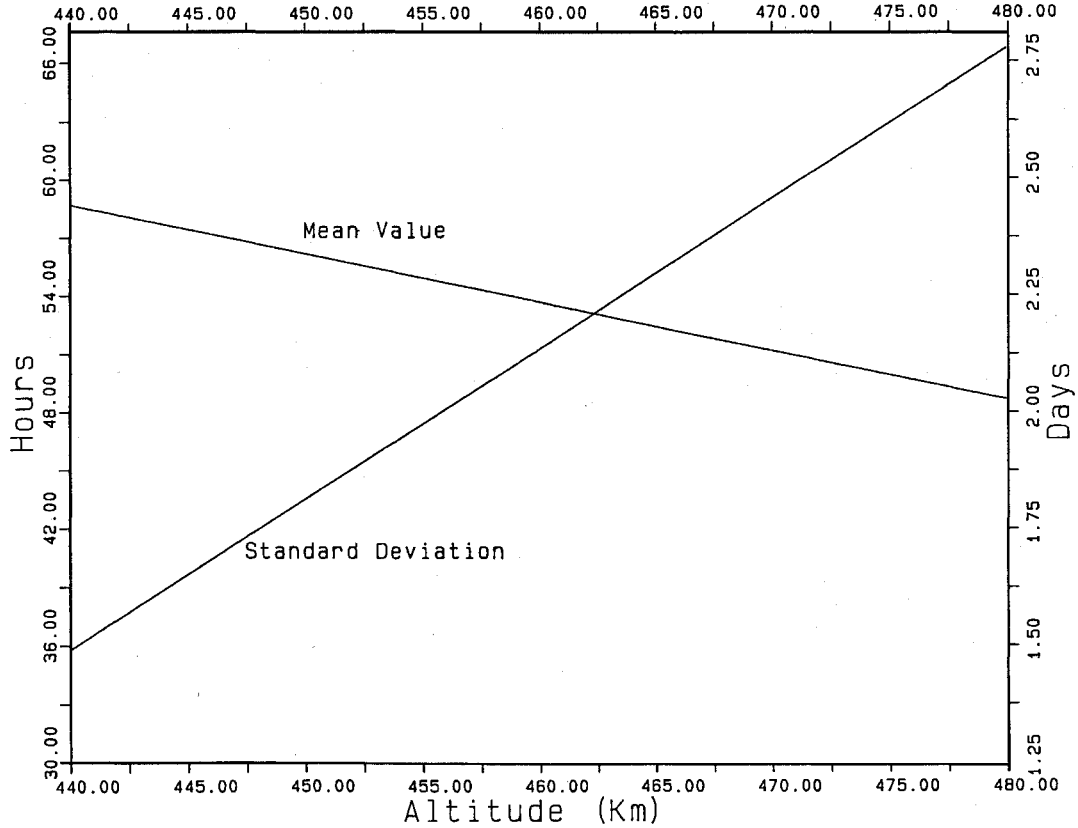

Fig. 2 Mean value and standard deviation between successive observations as a function of the Space Station altitude (antenna steering 15–45 deg).

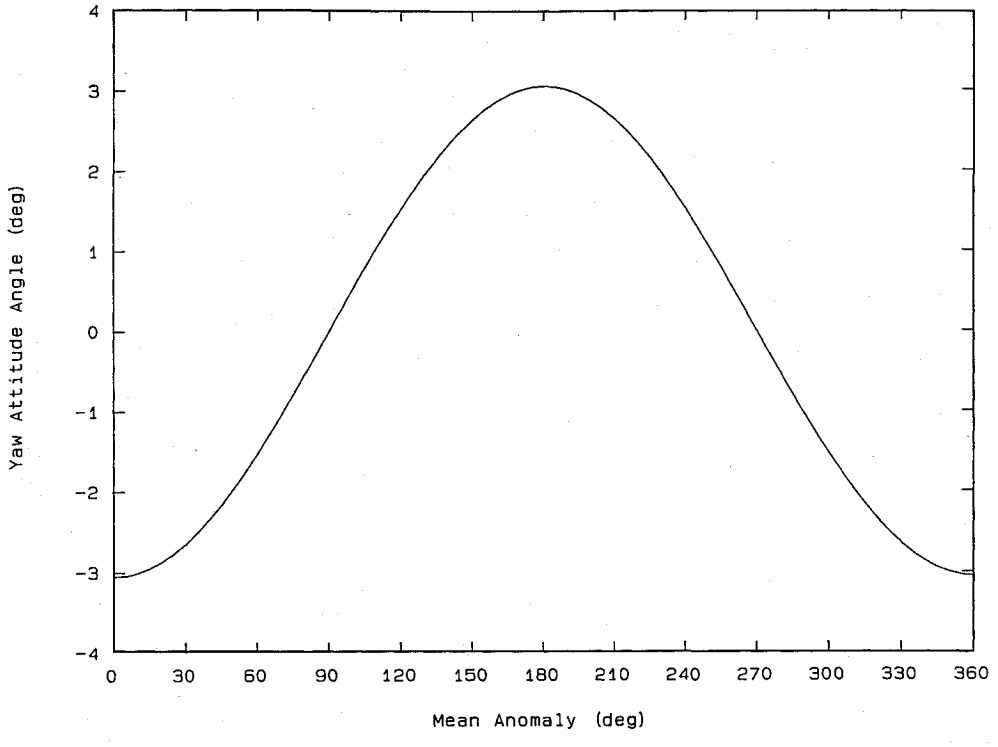

Fig. 3 Yaw attitude angle for minimum drag as a function of mean anomaly for the orbit with the repetition factor 892/59.

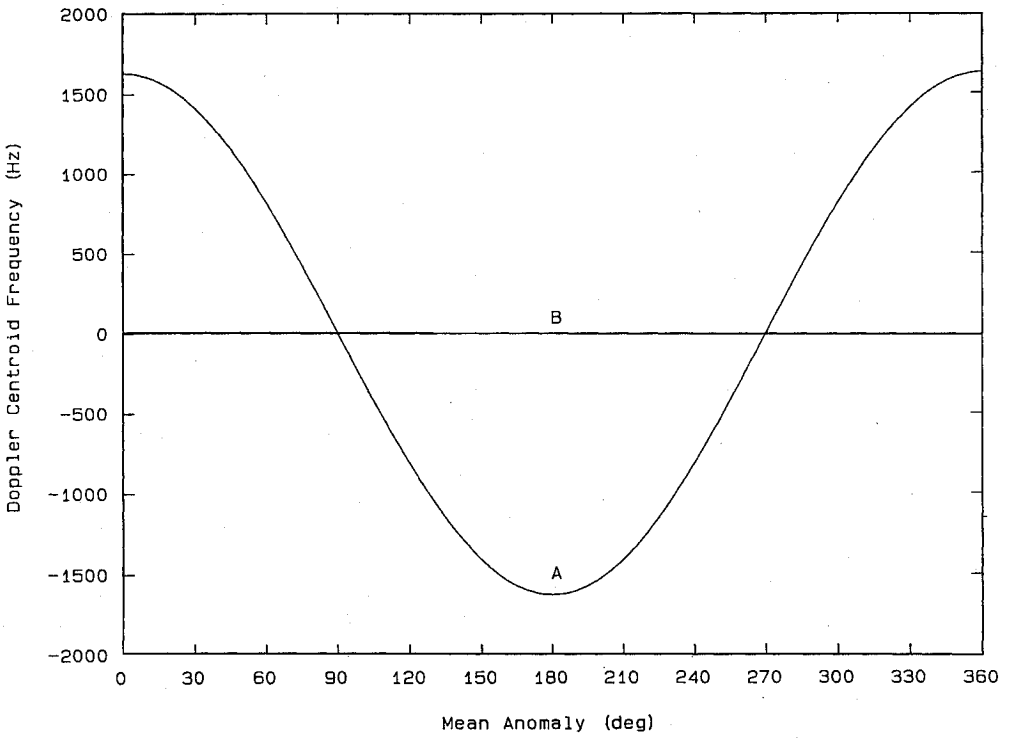

Fig. 4 Doppler centroid frequency for the T/R and the R/o antennas without yaw steering (A) and with yaw steering (B) as a function of mean anomaly for the orbit with repetition factor 892/89.

case, the SAR Doppler centroid frequency attains a zero value.[15] Although the yaw maneuver is not absolutely requisite, this property is relevant to improving image focusing because the range migration effects are strongly reduced.

The yaw attitude angle is a function of the mean anomaly and, if a circular orbit is considered, is given by

$$\gamma = \tan^{-1}\left(\frac{\sin i \cos\beta}{\omega/\omega_{\oplus} - \cos i}\right) \tag{7}$$

The required yaw attitude angle is in the range ±3 deg (Fig. 3).

The Doppler centroid frequency of the T/R antenna image can be expressed as follows:

$$f_D = -(2/\lambda)[(\dot{\boldsymbol{R}} \cdot \boldsymbol{R})/R] \tag{8}$$

For the R/o image a different return path must be considered, taking into account the baseline between the antenna foci.

The centroid frequency has been computed for both antennas and considering both the case with yaw steering and the case without

yaw steering (Fig. 4). As expected, if the yaw steering maneuver is adopted, the centroid frequency is zero also for the R/o antenna, because in the nominal case it is perfectly aligned along the local vertical of the T/R one. On the other hand, because of the target–antenna relative velocity along the orbit, a cosinusoidal curve is obtained when the yaw steering is not applied. Also in the latter case the Doppler centroid frequencies of the two antennas are practically coincident. This is due to the negligible difference between the look angles, as required to avoid baseline decorrelation.[2,13,16]

Then, the Doppler bandwidth was computed (Fig. 5), because it strongly influences the SNR, as will be shown in the following. Its value is about 1432 Hz for the various cases considered. The effects of the variation of the Earth surface tangential velocity as a function of latitude are evident when the yaw steering is applied. The slight difference between the Doppler bandwidths of the two antennas is due to the size of the SAR footprints, which depend on the radar altitudes. If necessary, this effect can be easily allowed for in the advanced SAR processor.

Tether Effects

Of course, a constant vertical baseline cannot be achieved during the stationkeeping phase of the mission. Therefore, it is necessary to evaluate the order of magnitude of tether-dynamics-induced perturbations on SAR Doppler properties and coverage.

In-plane, out-of-plane, and longitudinal low-frequency oscillations of the order of the orbital rate cause variations in the baseline that can be measured by using laser sensors or GPS antennas with adequate accuracy.[21]

Table 2 Mechanical and thermal characteristics of 1-km tether

Radius	5.0×10^{-3} m
Linear density	8.95×10^{-2} kg m^{-1}
Solar-radiation absorptivity	0.5
Thermal emissivity	0.75
Specific heat	2.5×10^{3} J kg^{-1} K^{-1}
Young's modulus	1.95×10^{10} N m^{-2}
Thermal expansion coefficient	-6.1×10^{-6} K^{-1}
Damping coefficient	0.05
Drag coefficient	3.0

As far as the high-frequency longitudinal oscillations are concerned, several authors have shown that adequate control laws can effectively damp their amplitudes.[22] To perform a quantitative evaluation of these contributions, a three-dimensional numerical model, based on the discretization of the system by means of lumped masses connected by massless springs and dashpots, has been used. The system orbital motion is described by the force- and energy-balance differential equations, the unknown quantities being the temperature and the components of the position and velocity vectors of each mass with respect to an inertial reference frame. The environmental perturbations considered are the force of gravity, including the second zonal harmonic of the gravity field; the aerodynamic forces; and the thermal effects on the tensional forces.[23] In particular, for each lumped mass, 1) the aerodynamic drag is evaluated considering the velocity of its center of mass relative to the rotating atmosphere, and 2) the tether thermal inputs are the solar radiation and the flux due to the atmospheric drag, whereas the only cooling process is the emitted radiation.

The computer simulation has been performed considering the end masses representing the Space Station (mass 401,883 kg, cross-sectional area 839.21 m^2) (Ref. 19), and the tethered subsatellite (mass 800 kg, cross-sectional area 1 m^2), and five lumped masses representing a nonconductive tether (Table 2). To evaluate the subsatellite cross-sectional area it has been assumed that the SAR antenna and the solar panels are along the spacecraft–atmosphere relative velocity, thanks to the yaw steering maneuver.

To allow for a more stringent case, no tether longitudinal and lateral oscillation control laws have been included in the computer runs. Table 3 summarizes the results of the simulation relevant to the proposed SAR application. In particular, it lists the standard deviations of the subsatellite antenna focus position and velocity vector components with respect to a Space Station antenna fixed

Table 3 Standard deviations of the R/o antenna position and velocity components, with respect to the T/R one, during stationkeeping phase of the mission[a]

x, m	y, m	Δz, cm	$\dot{x}$, mm/s	$\dot{y}$, mm/s	$\dot{z}$, mm/s
4	2	8	9	3	0.1

[a]The Δz component is computed with respect to the gravity-gradient-stabilized equilibrium position.

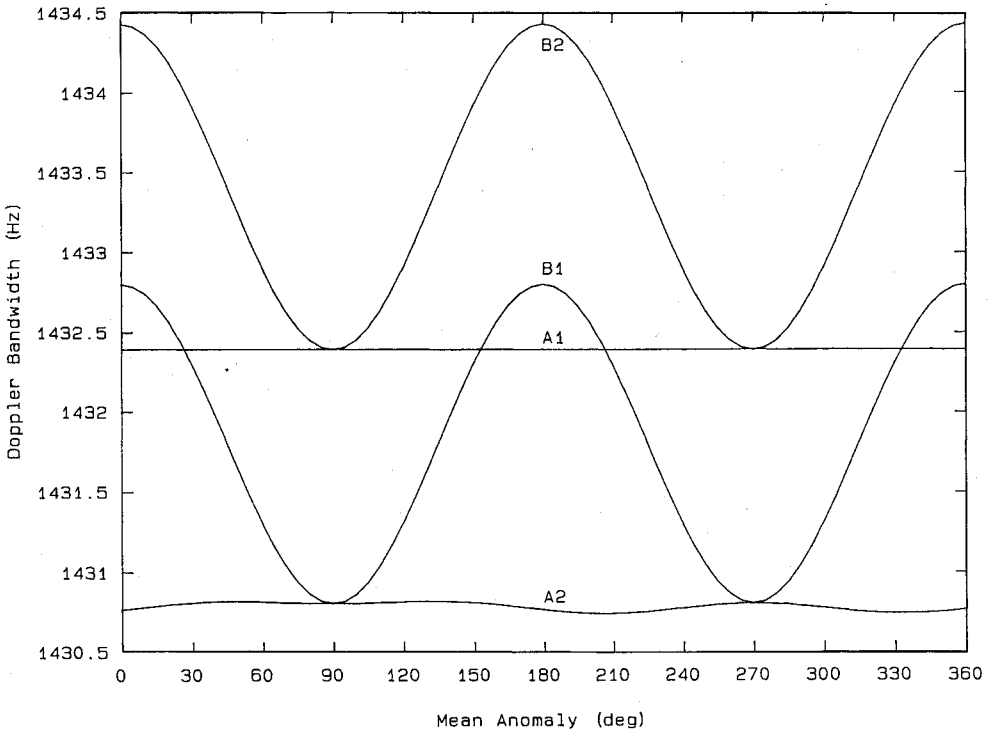

Fig. 5 Doppler bandwidth for the T/R (1) and the R/o (2) antennas without yaw steering (A) and with yaw steering (B) as a function of mean anomaly for the orbit with the repetition factor 892/89.

orbiting reference frame (whose origin is at the T/R antenna focus, z axis is coincident with its position vector and directed downward, y axis is perpendicular to the orbital plane, and x axis is directed forward). The variations of Doppler centroid frequency and Doppler bandwidth, which are caused by the standard deviations listed in Table 3, are of the order of 0.1 Hz, and, therefore certainly negligible. Also, the antenna footprint overlap is not affected by these small differences with respect to the unperturbed vertical configuration: the overlap between the T/R and the R/o 3-dB apertures is greater than 98%, even when tether perturbations are included.

Attitude Requirements

To define the attitude requirements of the tethered interferometer two aspects must be exploited. First, since the R/o antenna is passive, any pointing difference with respect to the T/R one will cause a reduction of the accessible area. Besides this essentially geometric problem, an additional radiometric aspect must be considered. If the two images are formed with different Doppler bandwidths because of the antenna misalignment, then the SNR of the interferogram and the height measurement accuracy of the system will be lowered. In the following we will derive the yaw and pitch requirements by considering the effects of misalignment on the height measurement accuracy, whereas the need of a satisfactory swath overlap will allow the roll requirement to be defined.

Definition of Yaw and Pitch Requirements

It has been shown that the focusing of both images can be carried out by using only one reference function.[24] In particular, a theoretical reference function can be obtained considering the T/R antenna flying at its nominal attitude. In this case, the actual Doppler parameters of raw data cause a decrease of SNR in the focused images and a consequent decrease of coherence in the interferogram. From the radar equation it is possible to derive the SNR as follows[25]:

$$\mathrm{SNR} = \frac{P_P G^2 \lambda^2 \sigma_0 A G_R G_A}{(4\pi)^3 R^4 N} \tag{9}$$

where G_A is the azimuth compression factor: $G_A = T_A \Delta W_A$. Introducing a constant C_1, we have

$$\mathrm{SNR} = C_1 \Delta W_A \tag{10}$$

By substituting Eqs. (4) and (10) in Eq. (3) and differentiating, we obtain the following equation that relates the common Doppler bandwidth to the height measurement accuracy:

$$\frac{\mathrm{d}\sigma_h}{\sigma_h} = \frac{\mathrm{d}(\Delta W_A)}{2\,\Delta W_A} \tag{11}$$

Therefore, if a height measurement error increase of the order of 5–10% is allowed (which is a satisfactory value in comparison with the other error sources[1,13,16]), the effective Doppler bandwidth decrease must be of the order of 10–20%.

To evaluate the attitude requirements quantitatively a computer simulation has been carried out. For each value of the mean anomaly along a Keplerian circular orbit, a Gaussian distribution of attitude angles with assigned standard deviation has been considered and the corresponding Doppler frequency and bandwidth distributions have been computed. As expected, the Doppler bandwidth of each antenna is not affected by attitude perturbations. In fact, the 3-dB aperture angles in both elevation and azimuth directions are quite large with respect to the achievable pointing errors, and the residual effect of the Earth ellipsoid is practically negligible. On the other hand, the Doppler centroid frequency is strongly affected by the yaw and pitch attitude angles (Table 4), whereas the roll angle only involves a variation of the antenna gain parameters.

As shown in Fig. 5, the nominal Doppler bandwidth is 1432 Hz. Therefore, if the proposed focusing technique is adopted and we consider 0.10 and 0.15 deg as standard deviations for pitch and yaw accuracy requirements, only $\Delta W_A = 1310$ Hz for the T/R antenna and $\Delta W_A = 1259$ Hz for the R/o antenna can be considered. In the latter case the narrower bandwidth is consequent to the mutual effects of the two antennas. These values yield a worst-case ratio $\mathrm{d}(\Delta W_A)/\Delta W_A = 12\%$.

Table 4 Root mean square error of Doppler centroid frequency with respect to the unperturbed case for yaw and pitch errors

Attitude angle: standard deviation, deg		Doppler centroid frequency: root mean square error, Hz	
Yaw	Pitch	T/R antenna	R/o antenna
0.50	——	263	265
0.20	——	105	106
0.15	——	79	80
——	0.50	455	459
——	0.10	91	92
0.15	0.10	122	122

Table 5 Swath-overlap mean value and standard deviation as a function of yaw, pitch, and roll errors

Attitude angle standard deviation, deg	Swath overlap	
	Mean value, %	Standard deviation, %
0.15 (yaw)	91.8	5.7
0.10 (pitch)	90.6	6.6
0.50 (roll)	79.7	15.0
0.25 (roll)	89.8	7.7
0.20 (roll)	91.8	6.2

Table 6 Yaw, pitch, and roll pointing accuracy requirements (1σ)

Yaw	Pitch	Roll
0.15 deg	0.10 deg	0.20 deg

The values listed in Table 4 have been calculated considering that the antenna is not rotating to perform the yaw steering maneuver. The same computation has been carried out also in the case of yaw steering, and no significant differences occurred.

Definition of Roll Requirement

The geometric constraint on roll angles is imposed by the need of an adequate swath overlap. To be consistent with the previous analysis, since the yaw (0.15 deg) and pitch (0.10 deg) standard deviations cause a swath overlap of about 90%, the roll standard deviation must guarantee the same value. Numerical simulations have shown that a roll standard deviation of the order of 0.20 deg is necessary (Table 5).

When all the attitude errors are considered, the mean value of swath overlap is of 84% with a standard deviation of 9%. The swath overlap calculations have been carried out for both the cases, with and without yaw steering, giving the same results. In conclusion, the required attitude system accuracy is not particularly stringent (Table 6).

Conclusions

This paper presents a spaceborne SAR interferometric system based on two tethered antennas and aimed at natural-disaster mapping and monitoring. Basically, the configuration consists of two antennas flying along parallel paths. The first is onboard the Space Station, whereas the second is carried by a small subsatellite tethered to the station. The vertical antenna separation required for accurate topographic mapping is obtained thanks to gravity gradient stabilization. High frequency of observations over areas hit by natural disasters is accomplished by electronic antenna range beam steering. Of course, the same results could be obtained considering mechanical antenna steering or a spacecraft roll rotation. In these latter cases the complexities in radar design and operation are replaced by a more sophisticated attitude control system.

From the quantitative point of view, the analysis was carried out in a wide range of Space Station orbit altitudes. It was found that the

repetition frequency increases from $\frac{1}{16}$ to $\frac{1}{2}$ day^{-1} when the potential beam width increases from the nominal 3-dB aperture to a steerable 15–45-deg beam. Furthermore, considering the Earth surface in the latitude range covered by the Space Station (±51.6 deg), in the mean 2 days are required to reobserve the same site, with a standard deviation of 2 days. This results is particularly interesting for natural-disaster mapping, because these areas are the most densely populated.

Then the attitude requirements were considered. Since the yaw and pitch angles mainly affect the Doppler bandwidth, the yaw and pitch accuracy were computed with the nominal height measurement accuracy reduced by about 10% with respect to the theoretical unperturbed attitude value. The roll requirement was designed assuming that the swath overlap decrease caused by roll attitude errors must not exceed that caused by yaw and pitch. The final result is that a medium level of attitude accuracy is required (yaw 0.15 deg, pitch 0.10 deg, roll 0.20 deg).

Acknowledgments

This work was carried out with financial contributions from the Italian Ministry for University and Research and the Italian Space Agency.

References

[1]Graham, L. C., "Synthetic Interferometer Radar for Topographic Mapping," *Proceedings of the IEEE*, Vol. 62, No. 6, 1974, pp. 763–768.

[2]Li, K., and Goldstein, R. M., "Studies of Multibaseline Space-Borne Interferometric Synthetic Aperture Radar," *IEEE Transactions on Geoscience and Remote Sensing*, Vol. 28, No. 1, 1990, pp. 88–97.

[3]Topographic Science Working Group, "Topographic Science Working Group Report to the Land Processes Branch, Earth Science and Application Division, NASA Headquarters," Lunar and Planetary Inst., Houston, TX, 1988, p. 64.

[4]TOPSAT Working Group, "Scientific Requirements of a Future Space Global Topography Mission," Italian Space Agency, Rept. Contract ASI-92-RS-S2, Rome, 1994, p. 85.

[5]Allen, C. T., "Interferometric Synthetic Aperture Radar," *IEEE Geoscience and Remote Sensing Society Newsletter*, Sept. 1995, pp. 6–13.

[6]Gabriel, A. K., Goldstein, R. M., and Zebker, H. A., "Mapping Small Elevation Changes over Large Areas: Differential Radar Interferometry," *Journal of Geophysical Research*, Vol. 94, No. B7, 1989, pp. 9183–9191.

[7]Massonet, D., Rossi, M., Carmona, C., Adragna, F., Peltzer, G., Feigl, K., and Rabaute, T., "The Displacement Field of the Landers Earthquake Mapped by Radar Interferometry," *Nature*, Vol. 364, No. 6433, 1993, pp. 138–142.

[8]Walter, L. S., "Application of Satellite Technology to Disaster Management," *Communication When It's Needed Most*, edited by D. Webster, Annenberg Washington Program in Communications Policy Studies of Northwestern Univ., Evanston, IL, 1989, pp. 74–93.

[9]D'Errico, M., Moccia, A., and Vetrella, S., "High Frequency Observation of Natural Disasters by SAR Interferometry," *Photogrammetric Engineering and Remote Sensing*, Vol. 61, No. 7, 1995, pp. 891–898.

[10]Penzo, P., and Johnston, M. D., "Mission Design for an Orbiting Volcano Observatory," *Journal of Spacecraft and Rockets*, Vol. 29, No. 4, 1992, pp. 502–507.

[11]Mattei, S., Vetrella, S., Moccia, A., Lane, A. L., Pieri, D. C., Abrams, M. J., and Bianchi, R., "Potential Observations with EURECA/VEXUVIO Imaging Spectrometer," *International Journal of Remote Sensing*, Vol. 15, No. 11, 1994, pp. 2175–2192.

[12]Crouch, D., Park, C., Kyrias, G., Strim, B., Lioy, S., Compton, G., Lorenzoni, A., and Conley, C., "An Update to Proposed Space Tether Applications for International Space Station Alpha," *Proceedings of the 4th International Conference on Tethers in Space* (prepared by Science and Technology Corp.), Vol. 3, Smithsonian Inst., Washington, DC, 1995, pp. 1501–1512.

[13]Rodriguez, E., and Martin, J. M., "Theory and Design of Interferometric Synthetic Aperture Radars," *IEE Proceedings—F*, Vol. 139, No. 2, 1992, pp. 147–159.

[14]Zebker, H. A., Farr, T. G., Salazar, R. P., and Dixon, T. H., "Mapping the World's Topography Using Radar Interferometry: The TOPSAT Mission," *Proceedings of the IEEE*, Vol. 82, No. 12, 1994, pp. 1774–1786.

[15]Moccia, A., Vetrella, S., and D'Errico, M., "Twin Satellite Orbital and Doppler Parameters for Global Topographic Mapping," *EARSeL Advances in Remote Sensing*, Vol. 4, No. 2, 1995, pp. 55–66.

[16]Moccia A., and Vetrella, S., "A Tethered Interferometric Synthetic Aperture Radar (SAR) for a Topographic Mission," *IEEE Transactions on Geoscience and Remote Sensing*, Vol. 30, No. 1, 1992, pp. 103–109.

[17]Goodman, J.W., "Statistical Properties of Laser Speckle Patterns," *Laser Speckle and Related Phenomena*, edited by J. C. Dainty, Springer–Verlag, New York, 1975, pp. 9–75.

[18]Duck, K. I., and King, J. C., "Orbital Mechanics for Remote Sensing," *Manual of Remote Sensing*, 2nd ed., Vol. 1, edited by R. N. Colwell, American Society of Photogrammetry, Falls Church, VA, 1983.

[19]European Space Agency—Council, "Interim Report on Utilisation Concept for Europe's Contribution to the International Space Station," ESA/C(94)60, June 14, 1994.

[20]Moccia, A., D'Errico, M., and Vetrella, S., "Synthetic Aperture Radar Interferometry by Means of Tethered Antennas," *Proceedings of the 4th International Conference on Tethers in Space* (prepared by Science and Technology Corp.), Vol. 3, Smithsonian Inst., Washington, DC, 1995, pp. 1631–1642.

[21]Bertiger, W. I., Lichten, S. M., and Katsigris, E. C., "A Demonstration of Sub-Meter GPS Orbit Determination and High Precision User Positioning," *IEEE Transactions on Aerospace and Electronic Systems*, Vol. 4, No. 2, 1989, pp. 16–25.

[22]Lakshmanan, P. K., Modi, V. J., and Misra, A. K., "Space Station Based Tethered Payload: Control Strategies and Their Relative Merit," *Tethers in Space, Toward Flight*, AIAA, Washington, DC, 1989, pp.166–177.

[23]Moccia, A., Vetrella, S., and Grassi, M., "Attitude Dynamics and Control of a Vertical Interferometric Radar Tethered Altimeter," *Journal of Guidance, Control, and Dynamics*, Vol. 16, No. 2, 1993, pp. 264–269.

[24]D'Errico, M., Moccia, A., and Vetrella, S., "Attitude Requirements of a Twin Satellite System for the Global Topography Mission," International Astronautical Federation, Paper 94-B.2.077, Oct. 1994.

[25]Ulaby, F. T., Moore, R. K., and Fung, A. K., *Microwave Remote Sensing*, Vol. 2, Addison–Wesley, Reading, MA, 1982.

I. E. Vas
Associate Editor